High-concentration organic solutions of poly(styrene-co-butadiene-co-styrene)-modified graphene sheets exfoliated from graphite

Yi-Tao Liu [a], Xu-Ming Xie [a,*], Xiong-Ying Ye [b]

[a] *Advanced Materials Laboratory, Department of Chemical Engineering, Tsinghua University, Beijing 100084, China*
[b] *Department of Precision Instruments and Mechanology, Tsinghua University, Beijing 100084, China*

ARTICLE INFO

ABSTRACT

A simple method is developed to produce high-concentration organic solutions of graphene sheets noncovalently modified with poly(styrene-co-butadiene-co-styrene) (SBS). Once exfoliated from natural graphite under sonication, the graphene sheets can be stabilized by SBS through the π–π stacking with the PS chains. The PS–graphene interaction is confirmed by DSC, since the glass transition temperature of the PS blocks increases by ∼8 °C, while that of the PB block remains unchanged. The content of SBS adsorbed on the graphene sheets is determined by TGA as ∼63 wt.%. Direct morphological observation is achieved by HRTEM, which reveals an amorphous polymer layer on the graphene sheets with individual polymer chains climbing on the edges. A freestanding, highly flexible film of SBS-modified graphene is prepared. The improved solubility of graphene in the organic solvents opens up a new opportunity for the solution-phase incorporation of graphene in the polymer matrices. The graphene/SBS composite has an excellent electrical conductivity with a percolation threshold of ∼0.25 vol.%. Besides, it is proven that SBS can also be adsorbed on chemically modified graphene and carbon nanotubes, demonstrating the versatility of the π–π stacking between the PS chains and the graphitic planes.

© 2011 Elsevier Ltd. All rights reserved.

1. Introduction

Graphene, a novel 2D carbon nanomaterial with superior electrical, thermal and mechanical properties [1–3], has recently provoked much research interest, just as fullerenes and carbon nanotubes (CNTs) did decades ago. Single- and few-layer graphene sheets have been successfully produced by, say, micromechanical cleavage of natural graphite [4], chemical vapor deposition [5], arc discharge [6], and epitaxial growth [7]. However, the low yield – a common characteristic of all these methods – restricts them to the laboratory-level fundamental studies only. For such applications as in high-performance graphene/polymer composites [8–10], graphene

has to be available in large amount and low cost. In this context, solution-based methods have been explored, aiming at the mass production of graphene.

Ruoff et al. succeeded in oxidizing natural graphite into graphene oxide (GO), and then reducing it into chemically modified graphene (CMG) with hydrazine hydrate [11]. In GO, the sp^2-hybridized carbon network is largely disrupted by bonding with such oxygen-containing groups as hydroxyl, epoxide and carboxyl. Therefore, GO is an electrical insulator. The reduction process eliminates most of the hydroxyl and epoxide groups, and the electrical conductivity is thus partly restored in CMG. The carboxyl groups, however, still occupy the edges of the CMG sheets, and facilitate further modifica-

tion with phenyl isocyanate [8], long-chain alkyl [12], polystyrene (PS) [13], etc. The integrity of the graphitic network is irreversibly damaged in this method, and CMG is proven by Raman spectroscopy to be highly defective [14,15].

To obtain high-quality, almost pristine graphene, several different ways have been worked out, using natural graphite, graphite intercalation compounds and expandable graphite as the starting materials. Dai et al. exfoliated graphene sheets from expandable graphite and stabilized them in the organic solvents through the π–π stacking with two conjugated polymers, poly(m-phenylenevinylene-co-2,5-dioctoxy-p-phenylenevinylene) [16] and 1,2-distearoyl-sn-glycero-3-phosphoethanolamine-N-[methoxy(polyethylene glycol)-5000] [17]. Similarly, an aqueous solution of graphene sheets was prepared from expandable graphite through the π–π stacking with 7,7,8,8-tetracyanoquinodimethane [18]. Penicaud et al., on the other hand, stirred a graphite intercalation compound, $K(THF)_xC_{24}$ (THF = tetrahydrofuran; x = 1–3), in N-methylpyrrolidone (NMP) to obtain a homogeneous colloidal suspension of graphene sheets [19].

It was found, interesting, that natural graphite can be directly exfoliated into graphene sheets in certain organic solvents under sonication [20,21]. The method is simple, and graphene with an electrical conductivity up to ∼6500 S/m can be obtained. However, the concentrations (0.16–8.5 mg/L) of the solutions as well as the yields (1–12 wt.%) are very low. Besides, many common nonpolar organic solvents, such as alkanes, benzene and its homologs, chloroform and THF, are extremely inefficient in dissolving the graphene sheets because of the weak affinity between the solvent molecules and graphene [22]. The poor solubility of graphene in the organic solvents, especially in the nonpolar ones, largely hinders its processability, thus a bottleneck to the incorporation of graphene in most of the polymer matrices. Recently the aqueous solutions of graphene, exfoliated from natural graphite and stabilized with sodium dodecylbenzenesulfonate [23], sodium cholate [24], 1-pyrenecarboxylic acid [25] and nonionic surfactants [26], were successfully realized. However, to produce organosoluble graphene sheets with high quality and productivity is still a fascinating challenge [27,28].

The hexagonal arrangement of the carbon atoms in an aromatic ring is isomorphic to that in a graphitic plane. Thus, the π–π stacking between the two is reasonably expected. It was reported that, by ourselves [29–31] and others [32,33], there is indeed an interaction between the PS chains and CNTs, which can be used to noncovalently modify CNTs with PS and PS-based copolymers. Note that CNTs modified with the PS homopolymer show limited improvement in the organosolubility, e.g., 66 mg/L in chloroform at best [31]. In contrast, nearly one-order-of-magnitude higher organosolubility is observed on CNTs modified with the PS-based copolymers [29,30]. It is believed that a PS-based copolymer is much more efficient in solubilizing CNTs in the organic solvents like a surfactant: the PS chains are selectively adsorbed on the CNT surfaces to compensate the inherent intertube van der Waals attraction, while the chains of the other component extend in the solvents to regulate the solubility.

Since theoretically a graphene sheet can be rolled up to form a CNT, or in other words, a CNT can be spread along its axis to form a graphene sheet, it is natural to extend the noncovalent modification strategy from CNTs to graphene. Compared with conjugated polymers, the PS-based copolymers can endow graphene with reasonable solubility in the organic solvents with a much lower cost. Compared with small molecules, surfactants and homopolymers, the abundant resources of PS-based copolymers can broaden the range of organic solvents for graphene. The solubility of graphene is often limited by that of the specific small molecule, surfactant or homopolymer adsorbed on it. However, in the case of a PS-based copolymer, once PS is adsorbed on graphene, a flexible choice of the other component can regulate the solubility of graphene in different organic solvents as well as its compatibility with different polymer matrices. Graphene can even be solubilized in the organic solvents or incorporated in the polymer matrices that are not compatible with PS only by regulating the other component in a PS-based copolymer. Here, we report a simple and inexpensive method to exfoliate graphene sheets from natural graphite and noncovalently modify them with one of the most widely used PS-based block copolymers, poly(styrene-co-butadiene-co-styrene) (SBS), endowing graphene with reasonable solubility in a wide variety of organic solvents.

2. Experimental

2.1. Materials and reagents

The natural graphite powder (particle sizes ⩽ 300 mesh; purity ⩾ 98.0%) was purchased from Sinopharm Chemical Reagent Co., Ltd. The linear SBS triblock copolymer (M_w = 117,000; PDI = 1.40) was purchased from LG Chemical. All the other chemical reagents employed in the experiments were purchased from Beijing Chemical Works, and used as received.

2.2. Sample preparation

In a typical run, 100 mg of natural graphite powder was dispersed in 100 mL of NMP by sonicating for 2 h. Then 100 mL of SBS/NMP solution (2 wt.%) was added slowly. The mixed solution was sonicated at ambient temperature for 6 h such that SBS was sufficiently adsorbed on the exfoliated graphene sheets to stabilize them. Note that shorter sonication time might lead to insufficient SBS adsorption, while longer sonication time might lead to too many defects on the graphene planes. The obtained suspension was centrifuged at 12,000 rpm for 90 min, and the top half of the supernatant was pipetted out. A black solid product, denoted SBS-adsorbed graphene (SBS-a-G for short), was collected through vacuum filtration with a polytetrafluoroethylene membrane, and thoroughly rinsed with chloroform and THF before vacuum drying. SBS-a-G was then dissolved in a wide spectrum of organic solvents. The solid samples of SBS-a-G for further characterization were obtained from its chloroform solution through vacuum filtration, and dried in vacuum.

For comparison, 100 mg of natural graphite powder was dispersed in 100 mL of NMP by sonicating for 8 h (without adding SBS). The obtained suspension was centrifuged at

12,000 rpm for 90 min, and the top half of the supernatant was collected. The solid samples of neat graphene were derived from this solution through vacuum filtration, and dried in vacuum.

To test the versatility of the SBS adsorption on the graphene sheets, we also employed CMG as the starting material. GO was synthesized from natural graphite powder by a modified Hummers method [34], and pre-dissolved in water to obtain an aqueous solution (2.5 mg/mL). Briefly, 10 mL of aqueous solution of GO was pipetted out and dropped into a conical flask, to which 90 mL of N,N-dimethylformamide (DMF) was added. Then, 10 μL of hydrazine monohydrate was added to the above solution, and the whole system was kept at 80 °C for 12 h such that GO was reduced into CMG [15]. Thereafter, the graphene solution was sonicated for 2 h, to which 100 mL of SBS/DMF solution (2 wt.%) was added dropwise. Note that rapidly adding the SBS/DMF solution might cause the precipitation of SBS due to the presence of water in the system. The mixture was sonicated for 6 h such that SBS was sufficiently adsorbed on the CMG sheets. A black solid product, denoted SBS-adsorbed CMG (SBS-*a*-CMG for short), was collected following the same protocol as outlined above.

2.3. Equipment and characterization techniques

Sonication was carried out in a KQ100DB ultrasonic bath of Kunshan Ultrasonic Instruments Co., Ltd. under 40 kHz and 100 W.

Centrifugation was performed in a TGL-20 M centrifuge of Shanghai Luxiangyi Centrifuge Instrument Co., Ltd. at 12,000 rpm.

Fourier transform infrared spectroscopy (FT-IR) was recorded on the solid samples in a Nicolet 560 spectrometer.

Raman spectroscopy was recorded on the solid samples in a Renishaw RM2000 spectrometer with 514 nm laser excitation.

Thermogravimetric analysis (TGA) was recorded on the solid samples in a Shimadzu DTG-60 from ambient temperature to 1000 °C (heating rate = 20 °C/min) in air. The air flow was 50 mL/min, and the sample mass was ~10 mg.

Differential scanning calorimetry (DSC) was recorded on the solid samples in a Shimadzu DSC-60 from −150 °C to 200 °C (heating rate = 10 °C/min) in nitrogen. The nitrogen flow was 30 mL/min, and the sample mass was ~5 mg.

Transmission electron microscopy (TEM) was performed in a JEOL JEM-1200EX operated at an accelerating voltage of 80 kV. The samples were prepared by dropping the solutions on carbon-coated holey copper grids and then drying them in vacuum.

High-resolution TEM (HRTEM) was performed in a JEOL JEM-2010 operated at an accelerating voltage of 120 kV. The samples were prepared by dropping the solutions on holey copper grids and then drying them in vacuum.

Atomic force microscopy (AFM) was performed in a Shimadzu SPM-9500 in the tapping mode. The samples were prepared by spin-coating the solutions on cleaned silicon wafers at 2000 rpm for 1 min and then drying them in vacuum.

3. Results and discussion

Although graphene is proven to be soluble in certain organic solvents, the concentrations (0.16–8.5 mg/L) are very low [20,21]. For example, when graphene is dissolved in NMP, one of the most "efficient" solvents ever reported, the concentration is only ~4.7 ± 1.9 mg/L. The value is much lower than that reported on single-walled CNTs [35]. The reason lies in the extremely large specific surface area of graphene, which induces a strong interlayer van der Waals attraction, and thus a high restacking tendency. However, after SBS is added during the sonication process, it can be adsorbed on the exfoliated graphene sheets and prevent them from restacking, as illustrated in Fig. 1. Therefore, graphene adsorbed with SBS has largely improved solubility in NMP. Fig. 2a shows a photograph of the NMP solutions of neat graphene (left) and SBS-*a*-G (right), which can give us a direct impression of the significant concentration difference between them. A TEM image of the NMP solution of SBS-*a*-G is presented in Fig. 2b. Large quantities of isolated SBS-*a*-G sheets can be clearly seen in the image.

Fig. 3 shows the FT-IR spectra of natural graphite, SBS-*a*-G and SBS. The FT-IR spectrum of natural graphite is featureless, in accord with that reported elsewhere [36]. In the FT-IR spectrum of SBS-*a*-G, the newly emerged peaks at 752 and 696 cm^{-1} are related to the mono-substituted benzene rings in the PS chains of SBS. The strong peak at 964 cm^{-1} is derived from the dominant trans-1,4-butadiene structure, while the weak one at 908 cm^{-1} from the minor 1,2-butadiene structure of the polybutadiene (PB) chains. The FT-IR spectra confirm the adsorption of SBS on the graphene sheets.

To further elucidate the interaction between the PS chains and graphene, we measured the glass transition temperatures, T_gs, of SBS and SBS-*a*-G. SBS, as an immiscible block copolymer, has two distinct T_gs, of which the lower one corresponds to the relaxation behavior of the PB block, while the
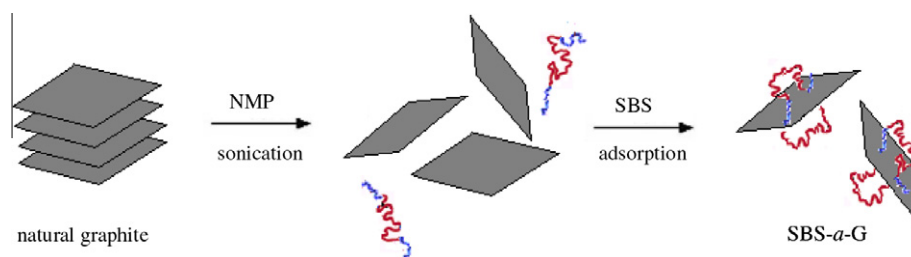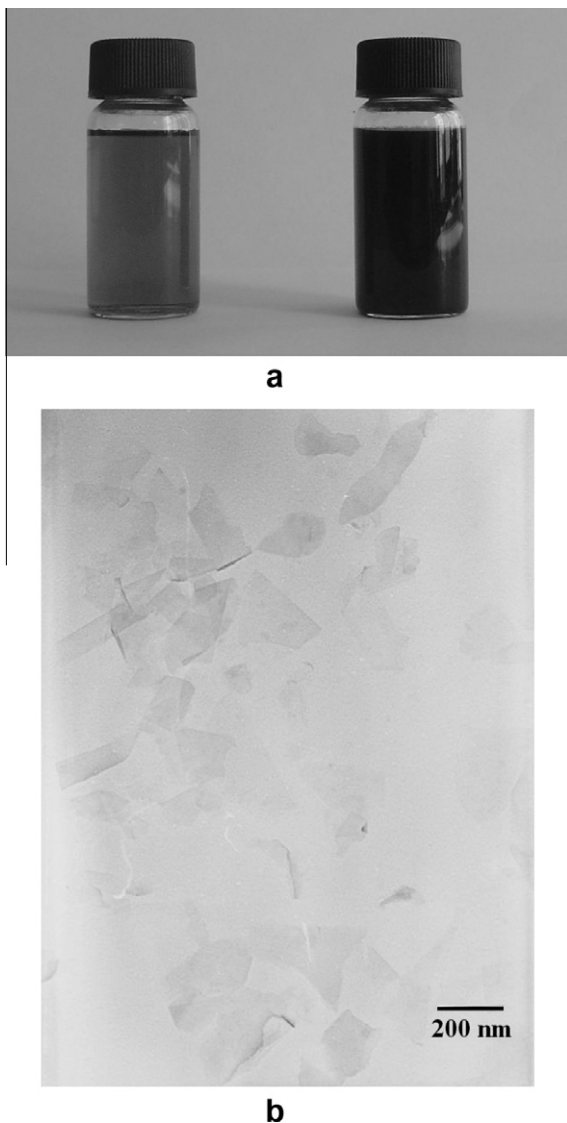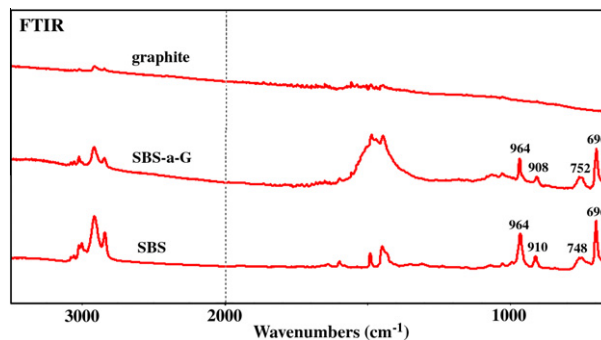

Fig. 1 – Scheme for the noncovalent modification of the exfoliated graphene sheets with SBS.
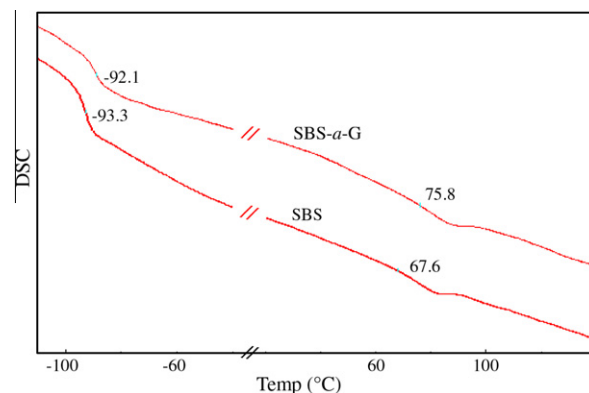
Fig. 2 – (a) Photograph of the NMP solutions of neat graphene (left) and SBS-*a*-G (right) and (b) TEM image of the NMP solution of SBS-*a*-G. All the samples in (a) were kept in ambient condition for more than 3 months before photographing.

Fig. 3 – FTIR spectra of natural graphite, SBS-*a*-G and SBS.

Fig. 4 – DSC curves of SBS and SBS-*a*-G. The results presented here are obtained in the second-round heating process to eliminate the thermal history of the samples.

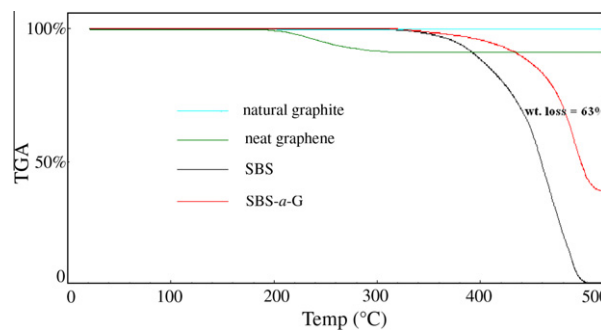Fig. 5 – TGA curves of natural graphite, neat graphene, SBS and SBS-*a*-G.

higher one to that of the PS blocks. Therefore, the T_g changes of SBS before and after being adsorbed on the graphene sheets, if any, can reflect the different extents to which the mobility of the PB and PS chains is confined by graphene. Fig. 4 shows the DSC curves of SBS and SBS-*a*-G. Clearly, the T_g change of the PB block is trivial. On the contrary, a remarkable T_g increase of ∼8 °C is witnessed on the PS blocks from SBS to SBS-*a*-G, implying a selective interaction between PS and graphene. A recent study on the solution-blended PS/single-walled CNT composite also found a T_g increase of 6–7 °C. Besides, it was claimed that the T_g increase does not change as the nanotube content increases from 1 to 30 wt.% [37]. Grafting PS to CMG [13] and multi-walled CNTs [38], however, led to much higher T_g increases, i.e., 15 °C and 35 °C, respectively. Hence, the change in T_g depends largely on the type of interaction between the PS chains and the graphitic sheets.

Fig. 5 shows the TGA curves of natural graphite, neat graphene, SBS and SBS-*a*-G. Natural graphite used in our experiment is thermally stable in air until ∼650 °C, above which a continuous weight loss occurs (∼50% at 900 °C). A similar result was reported by Kaner et al., who attributed the continuous weight loss at high temperature to the oxidation of the carbon atoms into CO_2 [39]. Different from that of natural graphite, the TGA curve of neat graphene has a small weight loss of 9% starting from ∼200 °C, which can be ascribed to the presence of the sparingly volatile solvent, NMP. A similar phenomenon was reported by Coleman et al. [20]. The thermal decomposition of neat graphene occurs at

~580 °C, from which a constant weight loss is observed. At ~800 °C, neat graphene is almost combusted completely. Natural graphite, however, has a weight loss of only ~30% at the same temperature. The lower thermal stability of neat graphene can be explained by the increased surface area, the decreased van der Waals interaction, the increased defect concentration, etc. The TGA curves of natural graphite and neat graphene up to 900 °C are provided in Supplementary material. In sharp contrast, SBS has a 100% weight loss at 500 °C, far below the initial decomposition temperature of neat graphene. The obvious difference in the thermal decomposition temperature of neat graphene and SBS helps us determine the content of the polymer in SBS-*a*-G to be ~63 wt.%. Note that the TGA curve of SBS-*a*-G does not have a small weight loss at relatively low temperature like that of neat graphene. This is because the solid sample of SBS-*a*-G was collected from its chloroform solution, and dried in vacuum before the TGA measurement. Since chloroform is a volatile solvent, there is little residual chloroform on SBS-*a*-G.

Raman spectroscopy is a powerful tool to characterize the carbon materials [40]. Generally, there are three common peaks, i.e., a D peak at ~1350 cm^{-1}, a G peak at ~1580 cm^{-1}, and a 2D peak at ~2700 cm^{-1}. The D peak is defect-related, and originates from the in-plane breathing mode of A_{1g} symmetry due to the presence of sixfold aromatic rings [41]. For the defect-free graphitic sheets, the D peak is invisible. The G peak corresponds to the E_{2g} mode, and is related to the vibration of the sp^2-hybridized carbon atoms in the graphitic sheets. The 2D peak is the second order of the D peak, and always present even when there is not a D peak because no defects are required for the activation of two phonons with the same momentum. The intensity ratio of the D and G peaks, I(D)/I(G), is often referred to indicate the quantities of defects in the carbon materials. Fig. 6 shows the Raman spectra of natural graphite and SBS-*a*-G (in the bulk state). The I(D)/I(G) ratio rises from 0.19 (natural graphite) to 0.32 (SBS-*a*-G), suggesting more sonication-induced basal plane defects and/or edge defects present in SBS-*a*-G. Here we stress that the I(D)/I(G) ratio of SBS-*a*-G is much lower than that reported
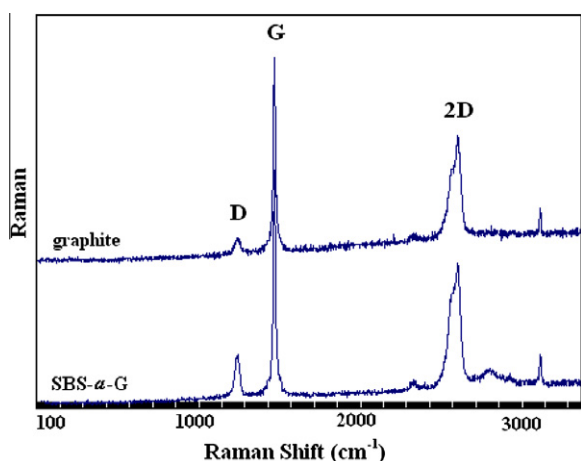

Fig. 6 – Raman spectra of natural graphite and SBS-*a*-G (in the bulk state).

on CMG [11,14,15], which is heavily and irreversibly damaged by the oxidation–reduction process.

We found that SBS-*a*-G was soluble in a wide variety of organic solvents that are compatible with SBS, and the solutions could withstand high-speed centrifugation (12,000 rpm, 90 min) without any visible precipitate (Supplementary material). The results indicate that the graphene sheets can be stabilized by SBS in the organic solvents, yielding high-concentration organic solutions. The reasonable solubility of SBS-*a*-G in the organic solvents opens up a new opportunity for the solution-phase graphene processing. It was also found that, interestingly, graphene nanoribbons with various widths and shapes could be produced by our method, and five representative ones are presented in Supplementary material.

HRTEM provides us with an ability to directly characterize the morphology of SBS-*a*-G, as shown in Fig. 7. Fig. 7a focuses on a single-layer SBS-*a*-G sheet. Seen from the figure, the surface of the single-layer SBS-*a*-G sheet is coated with an amorphous layer (presumably composed of SBS), which blurs the otherwise clearer image of highly crystalline graphene at the same magnification. Part of the graphene sheet's smooth edge is visible, while the rest is coated with the amorphous layer. A similar phenomenon was reported by Coleman et al., who found the ununiform coating of graphene sheets with a surfactant (sodium dodecylbenzenesulfonate) under HRTEM [23]. To further discriminate the SBS chains from graphene, we elaborately present the image of a multi-layer SBS-*a*-G sheet here (Fig. 7b). The surface of the multi-layer SBS-*a*-G sheet is also coated with a porous amorphous layer. Moreover, individual SBS chains extending from the amorphous layer can be clearly seen at the edge of the multi-layer SBS-*a*-G sheet. The HRTEM image directly proves the presence of SBS adsorbed on the graphene sheet. Previously we observed the uniform coating of double-walled CNTs with a PS-based graft copolymer [28]. In the case of graphene, however, its extremely large specific surface area is difficult for the uniform adsorption of polymer chains due to their high steric hindrance and low mobility. Therefore, a porous, fishing-net-like amorphous SBS layer is observed, with individual SBS chains extending out and climbing on the edge of the graphene sheets.

We further performed AFM on more than 70 isolated SBS-*a*-G sheets. The thickness of single-layer graphene exfoliated from natural graphite was reported to be 1–2 nm [20], being somewhat larger than the theoretical value (0.34 nm). This is because, among other reasons, the presence of the solvent effect. In contrast, more than 35% of the SBS-*a*-G sheets were found to have thickness of 3–3.5 nm. Occasionally, sheets with thickness of 1–2 nm were observed, which could be ascribed to neat graphene sheets without the SBS adsorption. Sheets with thickness of 2–3 nm were rarely seen. Therefore, 3–3.5-nm-thick sheets were the "thinnest" SBS-*a*-G sheets ever observed in AFM. Fig. 8 shows two representative SBS-*a*-G sheets with thickness of 3.42 nm and 3.07 nm. The diameters of the PS chains observed in Fig. 7b are >1 nm. If we assume SBS is adsorbed on each side of a graphene plane in a single-layer mode, we can deduce that the graphene sheets shown in Fig. 8 are ≤3 layers even when the solvent effect is not taken into consideration.
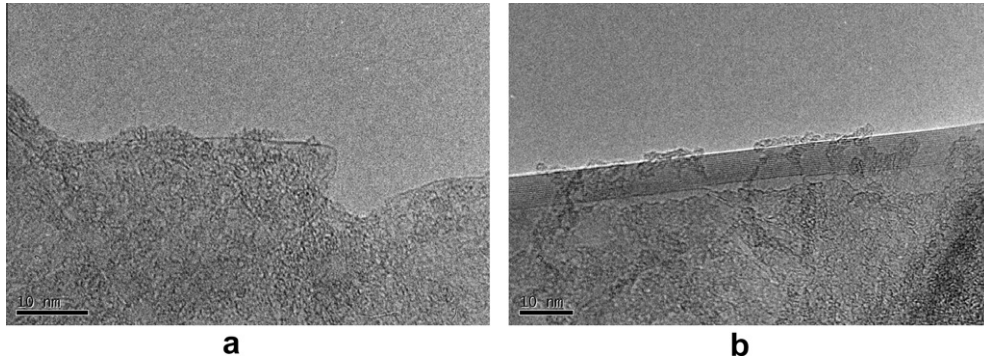
Fig. 7 – HRTEM images of (a) a single-layer SBS-*a*-G sheet coated with SBS and (b) a multi-layer SBS-*a*-G sheet coated with SBS. Note that individual SBS chains can be clearly seen at the edge of the multi-layer SBS-*a*-G sheet in (b).
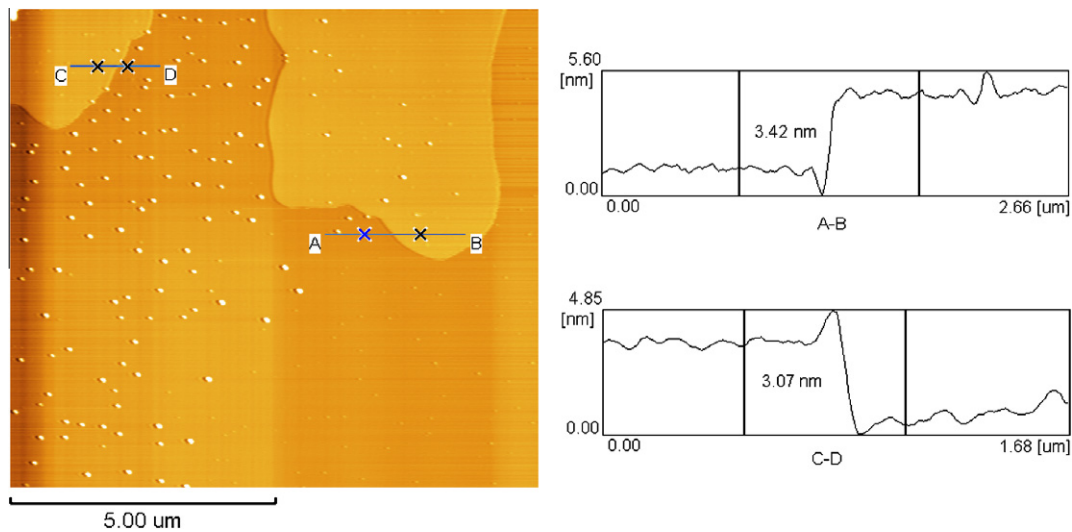

Fig. 8 – AFM image of two SBS-*a*-G sheets (left) and their corresponding height profiles (right).

Flexible and strong films of GO and CMG were frequently reported previously [42]. However, "graphene paper" made from a suspension of pristine graphene was porous and extre-mely fragile [43]. It was speculated that the functional groups in GO and CMG can tightly bind individual sheets together. Here we show a freestanding, highly flexible film of SBS-*a*-G
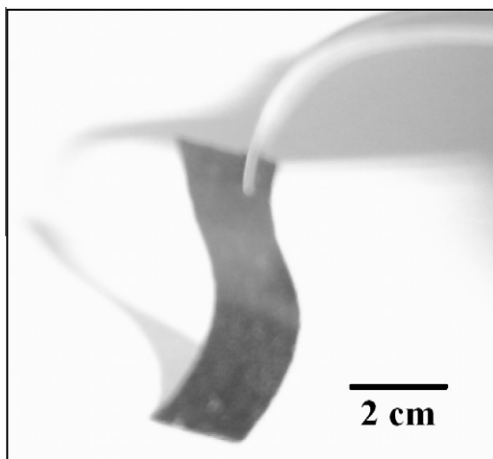
Fig. 9 – Photograph of a freestanding, highly flexible SBS-*a*-G film vacuum-filtered from the chloroform solution.
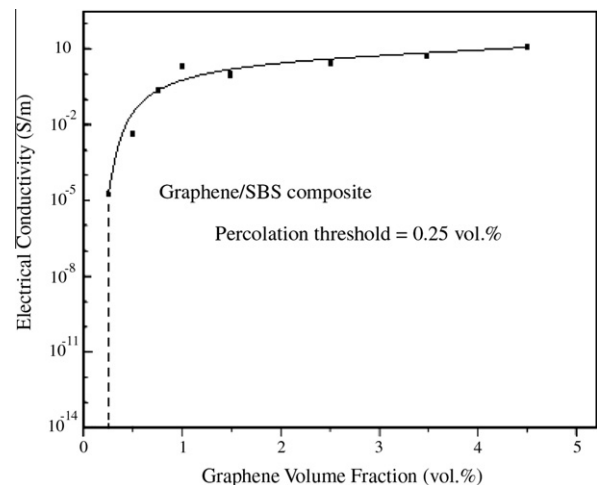
Fig. 10 – Electrical conductivity of the graphene/SBS composite as a function of the graphene volume fraction.

(Fig. 9) obtained by vacuum-filtering an SBS-*a*-G/chloroform solution. In this case, the graphene sheets are likely to be bound by the entangled SBS chains in between, resulting in enhanced flexibility and strength.

It is well known that when conducting filler is added to an insulating matrix, a so-called percolation phenomenon marking a rapid increase of the electrical conductivity occurs when the filler forms an infinite network of connected paths across the insulating matrix [8]. The percolation thresholds of graphene (GO, CMG) in such matrices as PS, polypropylene, epoxy resin, polycarbonate, poly(methyl methacrylate), thermoplastic polyurethane, polydimethylsiloxane, poly(vinylidene fluoride), polyamide 6 and styrene–isoprene–styrene triblock copolymer have already been studied [44]. However, to the best of our knowledge, the percolation characteristic of the graphene/SBS composite has not been touched. SBS, one of

the most widely used thermoplastic elastomers, is electrically insulating. When SBS-*a*-G is incorporated in the SBS matrix through solution blending, the percolation takes place at a graphene volume fraction of ∼0.25 vol.%, as shown in Fig. 10. Besides, a rapid, five-order-of-magnitude increase of electrical conductivity appears from 0.25 vol.% ($\sim3.5 \times 10^{-5}$ S/m) to 1.5 vol.% (∼1 S/m). After that the increase is relatively moderate until 4.5 vol.% (∼13 S/m), the highest graphene volume fraction tested in our experiment. The simple processing method and the excellent electrical performance of the graphene/SBS composite highlight a potential for industrial applications.

We also employed CMG as the starting material to test the versatility of the SBS adsorption on the graphene sheets. Fig. 11a shows the FT-IR spectrum of SBS-*a*-CMG thus obtained. As analyzed above, the peaks at 746 and 696 cm^{-1} are derived from the PS block of SBS, while those at 962 and 908 cm^{-1} from the PB block. The FT-IR spectrum confirms that SBS can also be adsorbed on the CMG planes. Fig. 11b shows the Raman spectra of GO and SBS-*a*-CMG. The increased $I(D)/I(G)$ ratio in the Raman spectrum of SBS-*a*-CMG (0.90), as compared to that of GO (0.83), suggests successful reduction/deoxygenation of GO into graphene [11]. Note that the $I(D)/I(G)$ ratio of SBS-*a*-CMG (0.90) is three times that of SBS-*a*-G (0.32) reported above, indicating much more defects in SBS-*a*-CMG caused by the oxidation–reduction process. Fig. 11c shows a TEM image of a single-layer SBS-*a*-CMG sheet. Previously we showed that SBS can be successfully adsorbed on CNTs [30,31] to improve their organosolubility. This result, combined with the findings in the present paper, demonstrate the versatility of the π–π stacking between the PS chains and the graphitic planes.

4. Conclusion
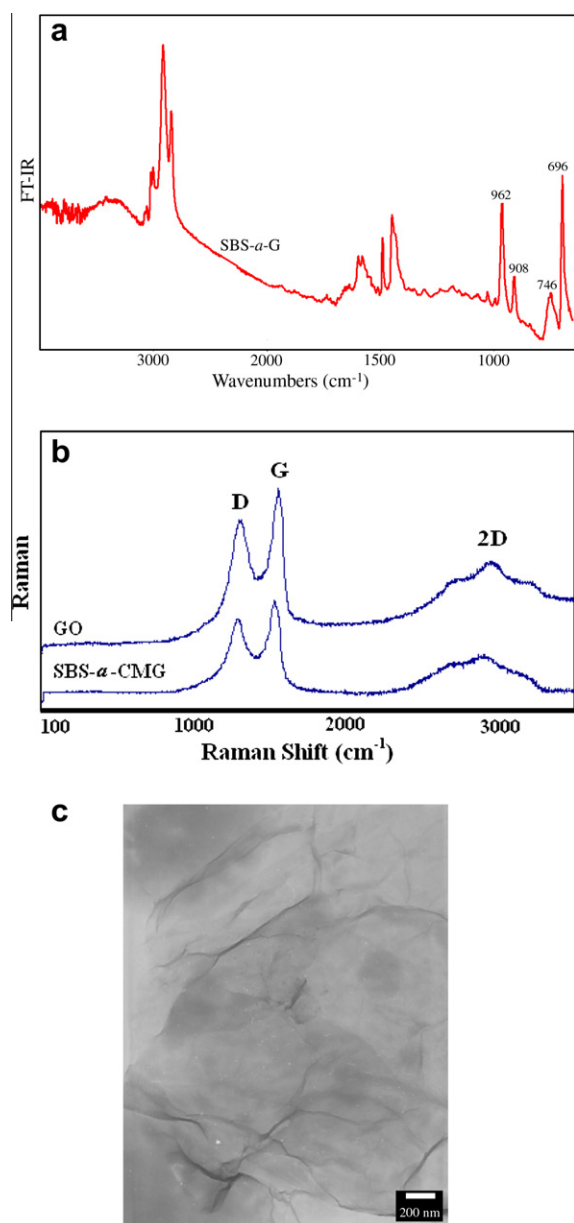
High-concentration organic solutions of graphene sheets have been produced from natural graphite through the π–π stacking with the PS chains of SBS. The noncovalent modification strategy retains the 2D lattice integrity of graphene, and imposes much fewer defects on the graphene planes as compared with CMG. The percolation characteristic of the graphene/SBS composite has been studied, and a relative low percolation threshold (∼0.25 vol.%) is observed. The high solubility of SBS-*a*-G in the organic solvents, as well as the excellent electrical performance may open up a new opportunity for the solution-phase production of high-performance graphene/polymer composites. Besides, the versatility of the π–π stacking between the PS chains and the graphitic planes has been demonstrated.

Fig. 11 – (a) FT-IR spectrum, (b) Raman spectrum and (c) TEM image of SBS-*a*-CMG.

Appendix A. Supplementary data

Supplementary data associated with this article can be found, in the online version, at doi:10.1016/j.carbon.2011.04.052.

REFERENCES

[1] Du X, Skachko I, Barker A, Andrei EY. Approaching ballistic transport in suspended graphene. Nat Nanotechnol 2008;3:491–5.

[2] Balandin AA, Ghosh S, Bao W, Calizo I, Teweldebrhan D, Miao F, et al. Superior thermal conductivity of single-layer graphene. Nano Lett 2008;8:902–7.

[3] Lee C, Wei X, Kysar JW, Hone J. Measurement of the elastic properties and intrinsic strength of monolayer graphene. Science 2008;321:385–8.

[4] Novoselov KS, Geim AK, Morozov SV, Jiang D, Zhang Y, Dubonos SV, et al. Electric field effect in atomically thin carbon films. Science 2004;306:666–9.

[5] Kim KS, Zhao Y, Jang H, Lee SY, Kim JM, Kim KS, et al. Large-scale pattern growth of graphene films for stretchable transparent electrodes. Nature 2009;457:706–10.

[6] Li N, Wang Z, Zhao K, Shi Z, Gu Z, Xu S. Large scale synthesis of N-doped multi-layered graphene sheets by simple arc-discharge method. Carbon 2009;48:255–9.

[7] Sutter PW, Flege J-I, Sutter EA. Epitaxial graphene on ruthenium. Nat Mater 2008;7:406–11.

[8] Stankovich S, Dikin DA, Dommett GHB, Kohlhaas KM, Zimney EJ, Stach EA, et al. Graphene-based composite materials. Nature 2006;442:282–6.

[9] Lu W, Lin H, Wu D, Chen G. Unsaturated polyester resin/graphite nanosheet conducting composites with a low percolation threshold. Polymer 2006;47:4440–4.

[10] Vadukumpully S, Paul J, Mahanta N, Valiyaveettil S. Flexible conductive graphene/poly(vinyl chloride) composite thin films with high mechanical strength and thermal stability. Carbon 2011;49:198–205.

[11] Stankovich S, Dikin DA, Piner RD, Kohlhaas KA, Kleinhammes A, Jia Y, et al. Synthesis of graphene-based sheets via chemical reduction of exfoliated graphite oxide. Carbon 2007;45:1558–65.

[12] Cao Y, Feng J, Wu P. Alkyl-functionalized graphene sheets with improved lipophilicity. Carbon 2010;48:1683–5.

[13] Fang M, Wang K, Lu H, Yang Y, Nutt S. Covalent polymer functionalization of graphene sheets and mechanical properties of composites. J Mater Chem 2009;19:7098–105.

[14] Eda G, Fanchini G, Chhowalla M. Large-area ultrathin films of reduced graphene oxide as a transparent and flexible electronic material. Nat Nanotechnol 2008;3:270–4.

[15] Park S, An J, Jung I, Piner RD, An SJ, Li X, et al. Colloidal suspensions of highly reduced graphene oxide in a wide variety of organic solvents. Nano Lett 2009;9:1593–7.

[16] Li X, Wang X, Zhang L, Lee S, Dai H. Chemically derived, ultrasmooth graphene nanoribbon semiconductors. Science 2008;319:1229–32.

[17] Li X, Zhang G, Bai X, Sun X, Wang X, Wang E, et al. Highly conducting graphene sheets and Langmuir–Blodgett films. Nat Nanotechnol 2008;3:538–42.

[18] Hao R, Qian W, Zhang L, Hou Y. Aqueous dispersions of TCNQ-anion-stabilized graphene sheets. Chem Commun 2008;6576–8.

[19] Valles C, Drummond C, Saadaoui H, Furtado CA, He M, Roubeau O, et al. Solutions of negatively charged graphene sheets and ribbons. J Am Chem Soc 2008;130:15802–4.

[20] Hernandez Y, Nicolosi V, Lotya M, Blighe FM, Sun Z, De S, et al. High-yield production of graphene by liquid-phase exfoliation of graphite. Nat Nanotechnol 2008;3:563–8.

[21] Hernandez Y, Lotya M, Rickard D, Bergin SD, Coleman JN. Measurement of multicomponent solubility parameters for graphene facilitates solvent discovery. Langmuir 2009;26:3208–13.

[22] Shih C-J, Lin S, Strano MS, Blankschtein D. Understanding the stabilization of liquid-phase-exfoliated graphene in polar solvents: molecular dynamics simulations and kinetic theory of colloid aggregation. J Am Chem Soc 2010;132:14638–48.

[23] Lotya M, Hernandez Y, King PJ, Smith RJ, Nicolosi V, Karlsson LS, et al. Liquid phase production of graphene by exfoliation of graphite in surfactant/water solutions. J Am Chem Soc 2009;131:3611–20.

[24] Green AA, Hersam MC. Solution phase production of graphene with controlled thickness via density differentiation. Nano Lett 2009;9:4031–6.

[25] An X, Simmons T, Shah R, Wolfe C, Lewis KM, Washington M, et al. Stable aqueous dispersions of noncovalently functionalized graphene from graphite and their multifunctional high-performance applications. Nano Lett 2010;10:4295–301.

[26] Guardia L, Fernández-Merino MJ, Paredes JI, Solís-Fernández P, Villar-Rodil S, Martínez-Alonso A, et al. High-throughput production of pristine graphene in an aqueous dispersion assisted by non-ionic surfactants. Carbon 2011;49:1653–62.

[27] Vadukumpully S, Paul J, Valiyaveettil S. Cationic surfactant mediated exfoliation of graphite into graphene flakes. Carbon 2009;47:3288–94.

[28] Geng J, Kong BS, Yang SB, Jung HT. Preparation of graphene relying on porphyrin exfoliation of graphite. Chem Commun 2010:5091–3.

[29] Liu Y-T, Zhao W, Huang Z-Y, Gao Y-F, Xie X-M, Wang X-H, et al. Noncovalent surface modification of carbon nanotubes for solubility in organic solvents. Carbon 2006;44:1613–6.

[30] Liu Y-T, Xie X-M, Gao Y-F, Feng Q-P, Guo L-R, Wang X-H, et al. Polymer-assisted assembly of carbon nanotubes via a template-based method. Carbon 2006;44:599–602.

[31] Zhao W, Liu Y-T, Feng Q-P, Xie X-M, Wang X-H, Ye X-Y. Dispersion and noncovalent modification of multi-walled carbon nanotubes by various polystyrene-based polymers. J Appl Polym Sci 2008;108:1737–43.

[32] Liao K, Li S. Interfacial characteristics of a carbon nanotube–polystyrene composite system. Appl Phys Lett 2001;79:4225–7.

[33] Wong M, Paramsothy M, Xu XJ, Ren Y, Li S, Liao K. Physical interactions at carbon nanotube–polymer interface. Polymer 2003;44:7757–64.

[34] Kovtyukhova NI, Ollivier PJ, Martin BR, Mallouk TE, Chizhik SA, Buzaneva EV, et al. Layer-by-layer assembly of ultrathin composite films from micron-sized graphite oxide sheets and polycations. Chem Mater 1999;11:771–8.

[35] Bahr JL, Mickelson ET, Bronikowski MJ, Smalley RE, Tour JM. Dissolution of small diameter single-wall carbon nanotubes in organic solvents? Chem Commun 2001:193–4.

[36] Liu N, Luo F, Wu H, Liu Y, Zhang C, Chen J. One-step ionic-liquid-assisted electrochemical synthesis of ionic-liquid-functionalized graphene sheets directly from graphite. Adv Funct Mater 2008;18:1518–25.

[37] Grady BP, Paul A, Peters JE, Ford WT. Glass transition behavior of single-walled carbon nanotube–polystyrene composites. Macromolecules 2009;42:6152–8.

[38] Shanmugharaj AM, Bae JH, Nayak RR, Ryu SH. Preparation of poly(styrene-co-acrylonitrile)-grafted multiwalled carbon nanotubes via surface-initiated atom transfer radical polymerization. J Polym Sci Part A: Polym Chem 2007;45:460–70.

[39] Viculis L, Mack J, Mayer O, Hahn HT, Kaner RB. Intercalation and exfoliation routes to graphite nanoplatelets. J Mater Chem 2005;15:974–8.

[40] Dresselhaus MS, Jorio A, Hofmann M, Dresselhaus G, Saito R. Perspectives on carbon nanotubes and graphene Raman spectroscopy. Nano Lett 2010;10:751–8.

[41] Pimenta MA, Dresselhaus G, Dresselhaus MS, Cancado LG, Jorio A, Saito R. Studying disorder in graphite-based systems by Raman spectroscopy. Phys Chem Chem Phys 2007;9:1276–91.

[42] Allen MJ, Tung VC, Kaner RB. Honeycomb carbon: a review of graphene. Chem Rev 2010;110:132–45.

[43] Geim AK. Graphene: status and prospects. Science 2009;324:1530–4.

[44] Kim H, Abdala AA, Macosko CW. Graphene/polymer nanocomposites. Macromolecules 2010;43:6515–30.